JME

Journal of Mining & Environment,
Vol.9, No.1, 2018, 1-18.
DOI: 10.22044/jme.2017.5975.1414

A new approach for assessing stability of rock slopes considering centroids of weak zones

A. Turanboy[1*], E. Ülker[2] and C.B. Küçüksütçü[3]

1. Mining Engineering, Seydişehir Ahmet Cengiz Engineering Faculty, Necmettin Erbakan University, Konya, Turkey
2. Computer Engineering, Engineering Faculty, Selçuk University, Kampüs, Konya, Turkey
3. BayE Information, Education and Consulting Ltd., Konya, Turkey

Received 7 July 2017; received in revised form 23 September 2017; accepted 23 September 2017
**Corresponding author: aturanboy@konya.edu.tr (A. Turanboy).*

Abstract
The intersection lines between discontinuity surfaces and their intersection points on the visible surfaces of any engineering structure may be the instability indicators. This paper describes a new approach to modelling the intersecting lines and points that would provide the first evaluation of any instability in an engineering structure characterized by the failure modes. In this work, the intersection lines were grouped according to their direction either in the reverse or in the same direction as the dip of the slope. Furthermore, the intersection lines are grouped according to various *ranges of the interior friction angle*, which can be selected by the users in a computer application developed for this work. The orientation of the intersecting lines and the location of the exposed intersection points are defined and assigned as the scatter points. These exposed points are clustered to determine the centroid locations. The K-means clustering is used in this step. Finally, all these analyses are integrated in a logical order, and the results obtained are used to assess the instabilities on the slope surface. Experiments are carried out on a rock cut along the Konya-Antalya (Turkey) highway, which is composed of limestone, to demonstrate the performance and results of the approach. The locations of the possible failure zones in the critical range of the interior friction angle are defined both visually and numerically along the slope. Experiments show that the proposed method is very useful and easy to implement and yields practical preliminary evaluation results pertaining to instabilities according to the basic failure modes.

Keywords: *Rock Mass, Failure Modes, Intersection Lines and Points, K-Means, Interior Friction Angles.*

1. Introduction

When addressing discontinuous rock masses, the properties of the discontinuities in the rock become of prime importance since they will determine, to a large extent, the mechanical behaviour of the rock mass [1]. These properties can be classified as geometric or non-geometric. The non-geometric properties are related to the mechanical behaviour of the infill material and the shear strength of the intact rock adjacent to the discontinuity, while the geometric properties define the fabric of the discontinuous rock mass [2]. In addition, the geometric features of a discontinuity affect the behaviour of the rock mass, particularly at shallow depths, much more strongly than the mechanical properties. However, the surface openings caused by engineering of the rock have a greater unit surface area than the underground openings. Therefore, surface excavations undergo failure more frequently, and are less stable than the underground ones.

Investigating the possible failures beforehand is highly important in the engineering decision-making and design process. Indeed, a visual explanation of failures is the initial step, and represents a useful tool in evaluation. A systematic and well-designed visual work also provides an effective way to arrive at a rapid solution to many problems faced by the managers

and engineers. The most important component that must be examined in a rock mass is discontinuities (e.g. faults, joints, beddings). The inhomogeneous and anisotropic nature of a rock mass is mainly attributed to its interior discontinuities. In these respects, a rock mass is an excellent object for visualization. The geometric properties of discontinuities have been extensively reported on by ISRM (1981) [3].

Discontinuities, which are distributed randomly and irregularly in a rock mass, are generally considered under the frameworks of the statistics and probability theories [4-6]. The main aim of these theories is to qualitatively and quantitatively evaluate the slope stability using the discontinuity and intact rock data.

The geometrical parameters, which include the dip, dip direction, orientation, spacing, and length of a discontinuity, are directly gathered from rock mass exposure or bore holes made inside a rock mass using several surveying techniques. These parameters are generally used to understand the statistical nature of the discontinuities and in the instability analyses. For example, the plotting and contouring of discontinuity orientations on stereonets have long been performed to determine prominent orientations for the kinematic analyses. Spherical projections are a method for representing a 3-D (three-dimensional) spherical data on a 2-D (two-dimensional) plane. The structural geologists often use a Schmidt stereonet (a Lambert equal-area projection of the lower hemisphere of a sphere onto the plane of a meridian). The equal-area projection preserves the intensity of points, although the shapes of projected groups (clusters) will vary according to their original position on the sphere. For equal-angle projections, large and small circles are projected as circular areas. Hence, a contour plot of a unimodal dataset, which exhibits circular contours when projected using equal-angle projection, indicates that the data is isotropic about their mean direction. More information on the spherical projections can be found in the works carried out by Hoek and Bray (1981) and Davis (2002) [7, 8].

The most important challenges in modelling rock mass are the geometrical representation of complex 3-D discontinuity systems and the existence of many variables in these heterogeneous structures. In discontinuity analyses, the discontinuities are commonly represented in a reduced form either as line segments or as points. The line segments are defined by the connection of two intersection points in 2-D or ellipses in a 3-D space. Discrete fracturing Network (DFN) modelling, originally proposed by Dershowitz and Einstein (1988) [9], is a method for representing the fracture characteristics. The DFN models considered include those based on geological mapping, stochastic generation, and geomechanical simulation [10]. The simulated line segments and points are the main inputs for the construction of the DFN models. These models have been used in mining applications, primarily for kinematic analyses of rock slopes in open and underground excavations and to estimate the rock mass strength, fragmentation, anisotropic rock mass deformability, pore pressure distribution, and fluid connectivity of media.

Another modelling approach is the use of a stochastic network model, which is generated by marked point processes that incorporate the most significant fracture characteristics [11-14]. The use of marked point processes has proved to be an effective means of developing the stochastic fracture models [13]. In this approach, the fracture locations, orientations, and shapes are represented by points near the centre of 2-D shapes or the centroid of 3-D shapes. The resulting fracture intersection databases can be used for further applications such as the statistical and spatial analyses of intersections and, in particular, fluid-connectivity analysis.

Many applications of cluster analysis have been used to solve the practical engineering problems. The clustering analysis methods such as K-means and fuzzy K-means have been widely used to identify discontinuity sets and characterize their orientation. In these methods, the resulting clusters, which consist of points representing discontinuity properties, can also be visualized by a stereonet representation of the facet's poles. Fuzzy clustering is based on dividing the clustered data points in the transformed space into k subsets using the fuzzy K-means algorithm. Then the computed degrees of membership of points in each cluster in the transformed space are assigned to their corresponding points in the original space of discontinuity orientations [15].

An alternative method for the characterization application is the semi-automatic identification of discontinuity sets using the kernel density estimation (KDE). 3-D data is recorded in the field, and a series of algebraic equations are used for the calculations. The principal datum used in KDE is the normal vector of discontinuity planes [16]. These methodologies involve large amounts of data about any rock block formed by

discontinuities such as their scattered pole densities, the dominant directions of any failure, the identification of discontinuity set numbers, and the statistical properties of discontinuity sets. In the work carried out by Turanboy (2016), the direct intersection points were used as the primary data and mapped with 2-D KDE intensities of these intersection points to identify weak zones [17].

With the development of remote sensing technologies such as LIDAR (light detection and ranging) and photogrammetry, stochastic modelling of fractures in rock masses based on point density estimation (using Fisher, KDE, K-means, fuzzy K-means clustering) has become widespread in the recent years. The general purpose of this estimation method is to construct a model that best describes the underlying point density structure of a dataset and the discontinuity characteristics represented by field data. In these techniques, the clustering and mapping of data are the main steps, and a large amount of data related to discontinuities and rock faces can be semi-automatically or automatically. A number of recent works have implemented these techniques to collect and analyse the discontinuity data, for example, to identify discontinuity orientations [16,18-24], determine roughness [25-27], conduct spacing analyses [28-30], evaluate persistence [26, 31-32], and determine slope instabilities [24, 33-36].

A structurally-controlled instability refers to the phenomenon in which blocks formed by discontinuities may be free to either fall or slide from the excavation periphery under a set of several forces, usually due to gravity. As a basic method, the kinematic analysis is used to analyse the potential of the various modes of rock block failures that occur due to the presence of unfavourably-oriented discontinuities. Several works have extensively examined the possibility of failure according to the corresponding failure modes [7, 37-44]. The kinematic feasibility tests assess the probabilities of different failure mechanisms based on the discontinuity orientations with respect to the slope orientation, and by constructing rock failure susceptibility maps, three fundamental kinematic mechanisms of instability were considered by Hoek and Londe (1974) [45]: *plane failure, wedge failure, and toppling failure*. The analysis of rock block stability due to these failure modes was verified using the stereo-graphical methods proposed by Matheson (1983) [46]. In addition, several geometric conditions were introduced to consider the kinematic feasibility of these failure modes in detail [7 and 44].

Various approaches and theories have also been developed with respect to the geometric approach to examine the nature of a rock mass. For example, the block theory [41] is a comprehensive and rigorous approach that involves identifying removable blocks, determining potential failure modes, and assessing stability by 3-D geometric characterization of a rock mass. The main purpose of the block theory is to analyse the finiteness, removability, and mechanical stability of various rock blocks under different engineering conditions by analysing the dip angles, dip directions of discontinuities, interior friction angles, and direction of the active resultant force. The spherical projection and block theory have also been used both in the practical and detailed numerical analysis as descriptive tools for the geometric characterization of discontinuities in 2-D and 3-D spaces.

However, these methodologies are too complex and time-consuming, and offer a limited information or require additional studies regarding the grouping analysis of the failure modes and the locations of possible failures for rock slopes.

In this paper, a modelling approach is proposed to conduct a preliminary assessment for the stability analysis of rock slopes. The approach is a combination of the visualization and statistical methods. In developing the proposed model, the linear geometry concepts and the trigonometric identities were considered, and an interconnected and hierarchical approach was embraced. Essentially, it was assumed that failures were resisted only by surface friction. Additionally, different user-defined ranges (five ranges were selected in the experimental analyses) of interior friction angles of discontinuity surfaces were considered to demonstrate the feasibility of the results of the suggested approach. In the proposed model, the day-lighted intersection points on free surfaces were directly used as the main data for the statistical analysis. Furthermore, the intersection lines were generated from the calculated intersection points. Then these two derived secondary data were integrated into the well-known main conditions for *plane*, *wedge*, and *toppling failures*. Thus rock failures were classified on free surfaces, and their locations were specified. Furthermore, the failure conditions were evaluated over various ranges of interior friction angles.

This paper is organized as what follows. In Section one, the importance of the problem is

emphasized and the literature studies are summarized. The proposed approach is presented in detail in Section two. In Section three, the successful performance of the proposed method is demonstrated using a field study. Finally,the conclusion section of the paper presents an assessment of the results.

2. Methodology

The tools used in the conceptual model and the developed approaches are presented hierarchically.

2.1. Background

In general, several geometric conditions have been introduced to consider the kinematic feasibility of the failure modes. The main ones that are related to the failure modes can be summarized as follow:

1) *Plane failure:* Release surfaces must be present to define the lateral slide boundaries; the dip of the sliding plane is less than the dip of the slope surface in the same direction; the intersection line must daylight on the excavation and the upper slope surface (Figure 1a).

2) *Wedge failure:* Two intersecting discontinuities occur, both of which dip out of the cut slope at an oblique angle; the dip of the intersection line is less than the dip of the slope surface, and in the same direction; the dip of the slope must exceed the dip of the line of intersection of the wedge forming two discontinuity planes; the intersection line must daylight on the excavation and upper slope surface (Figure 1b).

3) *Toppling failure:* Goodman and Bray (1976) [47] have described a number of different types of toppling failures that may be encountered in the field including flexural toppling, block toppling, and block-flexure toppling; blocks are formed by discontinuities dipping steeply into the excavation or upper slope surfaces, combined with cross discontinuities (release surfaces); the dip of the intersection line is less than the dip of the slope surface, and in the opposite direction; the dip of the toppling surface is greater than 70°; the intersection line must daylight on the excavation and/or upper slope surface [47-48]. Block toppling occurs where narrow slabs are formed by joints dipping steeply into the face, combined with flatter cross-joints. The cross-joints provide release surfaces for rotation of the blocks. In the most common form of block toppling, the blocks, driven by self-weight, rotate forward out of the slope. Toppling failure is a more complex phenomenon; whether the rock block is stable depends on the ratio between the base length (b) - the height of rock blocks (h) and the dip angle of the sliding surface (ψ_t) - friction angle of the sliding surface (ϕ). The following instability and stability conditions have been reported by Goodman and Bray (1976) [47], De Freitas and Watters (1973) [49], and Owen et al. (1998) [50]:

1) $\psi_t > \phi$ and $b/h > \phi$ (sliding condition (1));

2) $\psi_t > \phi$ and $b/h < \phi$ (sliding and toppling condition (2));

3) $\psi_t < \phi$ and $b/h < \phi$ (toppling condition (3)); and

4) $\psi_t < \phi$ and $b/h > \phi$ (stable condition (4)).

where, ψ_{fi}, ψ_i , and ϕ are the dip angle of the slope, dip angle of the discontinuity surface or line, and friction angle of the discontinuity surface, respectively (Figure 1c). In the modelling study, rotational sliding, overturning, and flexural slip toppling were not considered. Only flexural toppling, block flexure, and block toppling were considered.

In this work, to assess the likelihood of such failures, analyses of the kinematic admissibility of potential failure blocks that intersect the slope face(s) (excavation and upper slope faces) were performed.

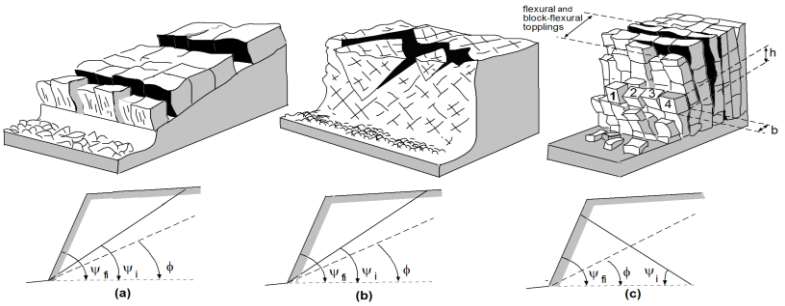

Figure 1. Main failure modes and their geometric parameters used in model: a) plane failure; b) wedge failure; c) toppling failure (flexural, block-flexure toppling, block toppling): sliding (1), sliding-toppling (2), toppling (3), stable condition (4) (adapted from Owen et al. (1998) [50]).

2.2. Survey techniques and scan-line survey

In this work, the primary raw data was the dip, dip direction angles of discontinuities, spacing, height of scan-lines, and dimensions of the experimental rock mass. The derived secondary data was the dip angle of the intersection lines inside the rock mass and the coordinates of the intersection points exposed on visible rock surfaces. The primary data was recorded simply by applying the basic scan-line technique, which consists of the directional and qualitative measurements of rock discontinuities [51, 52]. This data was recorded along a horizontal line in the field study. The visualized secondary (extended) data was derived from the primary raw data.

2.3. Parametric equations and 3-D computations

In the proposed approach, the first step is to describe the intersection points and lines, which are boundaries of the *in situ* polyhedral rock block, using the analytical geometry rules. These components are the secondary data used directly to create the model. The basic parameters of the model were calculated based on the intersection points of two line segments from a parametric form in a 3-D Cartesian coordinate system, and they were then connected systematically.

Assume that two points, $P_1 = (x_1, y_1, z_1)$ and $P_2 = (x_2, y_2, z_2)$, are given. Let P_1 and P_2 lie on two different lines, and $P_3 = (x_3, y_3, z_3)$ is the intersection point of these lines. In this case, the parametric forms of the two lines on P_1 and P_2 can be given by Equation 1. The intersection point of the two lines can be determined using the simultaneous equation method.

$$\begin{aligned} x_1 + \lambda \cos a_1 &= x_2 t \cos a_2 = x_3 \\ y_1 + \lambda \cos a_1 &= x_2 t \cos a_2 = y_3 \\ z_1 + \lambda \cos a_1 &= x_2 t \cos a_2 = z_3 \end{aligned} \quad (1)$$

where λ and t are the linear coefficients ($0 \leq \lambda \leq 1$ and $0 \leq t \leq 1$) and α is the angle measured clockwise relative to the x-, y-, and z-axes. The intersection point of the two lines is solved as (x_3, y_3, z_3). These equations are calculated for both the excavation and upper surfaces of the rock slope to determine the coordinates of the intersection points. The derived intersection points are also used to calculate the intersection lines inside the rock mass. Thus all intersection points, lines, and their spatial properties can be investigated easily. More information about the calculation of intersection points can be found in the work carried out by Turanboy and Ülker (2008) [53].

Another aspect of the model is that the discontinuities are assumed to be linear and infinite such that the free surfaces of the rock slope resemble *the 2-D trace plane* described by Dershowitz and Einstein (1988) [9]. In this work, to simplify the complexity of the structure, a series of reduction processes were performed for day-lighted polyhedral rock blocks regardless of the failure mode (wedge, planner or toppling). The intersection lines in the rock mass and day-lighted points of their lines on excavating surfaces represent the rock blocks. In addition, they are used in the 3-D visualization and statistical processes. Since any failure begins at the intersection points and proceeds along the intersection lines, it is assumed that any intersection point that belongs to any rock block occurs at the lowest location on the excavating surface. Thus each rock block can be modelled with polygons, and all intersection points on the excavating surface can be modelled. The logic is that the intersection lines are described in two different directions, which were handled separately as the intersection lines that are oriented in the reverse direction relative to the slope direction and the intersection lines that are oriented in the same direction as the slope direction. The same basic classification was performed for the intersection points on free surfaces in the model. A representative *2-D trace plane* on the excavation surface is shown in Figure 2.

2.4. Design of database and algorithmic structure of problem

There are 7 tables in the designed database, as shown in Figure 3. All data are stored in the database. First, an *Information System* must be created. This system includes the orientation parameters (dip, dip direction, location, and spacing) that belong to discontinuities and the representing prism. A unique identifying number (ID) for each rock mass is defined, and the associated data is classified based on this ID. This *Information System*, named "*The Discontinuity Input Table*", was used for the calculations performed in this work.

The next table is *The Mass Table*. It contains the outcrop, width, length, and height of the representing prism, and the height of the scan-line. These values must be provided as parameters, and the dimensions must be chosen by the user. In *The Discontinuity Input Table* and *The Mass Table*, the representing prism and discontinuity data are taken into account separately [53], and these two tables contain the primary data. Other tables store the calculation results and the secondary data.

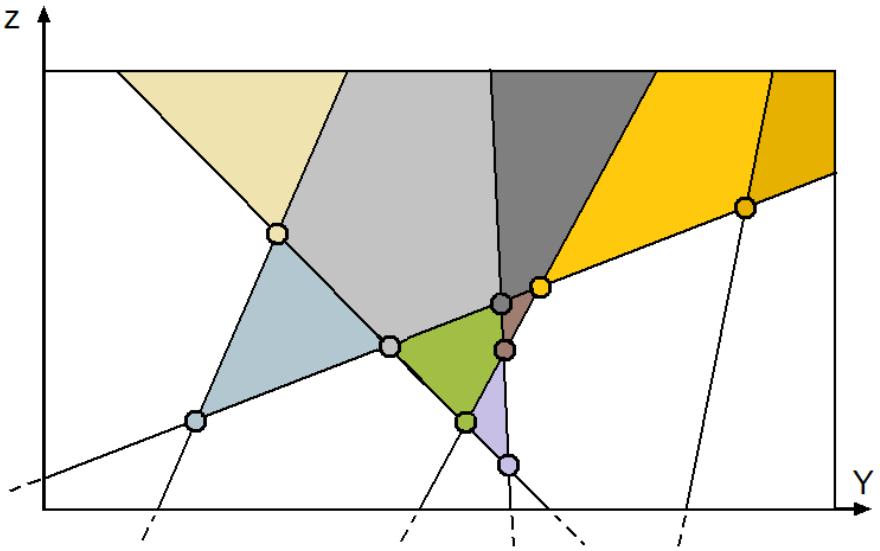

Figure 2. Excavating surface represented by 2-D trace plane. Each polygon is identified by intersection point at lowest location. Polygons and intersection points that are shown in the same colour belong together.

The intersection points on outcrop	
The probable intersected discontinuities	String
The number of intersection points on outcrop	Integer
The X-coordinate value of the point #1	Double
The Y-coordinate value of the point #1	Double
The Z-coordinate value of the point #1	Double
The X-coordinate value of the point #2	Double
The Y-coordinate value of the point #2	Double
The Z-coordinate value of the point #2	Double

The discontinuity input	
Rock mass id	Integer
Discontinuity id	Integer
Dip	Double
Dip direction	Double
Spacing	Double

The mass table	
Rock mass id	Integer
Outcrop	Integer
Scanline height	Double
Depth (size along X axis)	Double
Width (size along Y axis)	Double
Height (along Z axis)	Double

The intersection points on upper surfaces	
The probable intersected discontinuities	String
The number of intersection points on upper surface	Integer
The X-coordinate value of the point #1	Double
The Y-coordinate value of the point #1	Double
The Z-coordinate value of the point #1	Double
The X-coordinate value of the point #2	Double
The Y-coordinate value of the point #2	Double
The Z-coordinate value of the point #2	Double

The vertex points of discontinuity surface	
Discontinuity id	Integer
Number of vertices of the discontinuity	Integer
The axis of the discontinuity surface	String
The X-coordinate value of the point #1	Double
The Y-coordinate value of the point #1	Double
The Z-coordinate value of the point #1	Double
...	
The X-coordinate value of the point #6	Double
The Y-coordinate value of the point #6	Double
The Z-coordinate value of the point #6	Double

The intersection points on upper surfaces	
The probable intersected discontinuities	String
The surface information of the intersection point #1	String
The X-coordinate value of the point #1	Double
The Y-coordinate value of the point #1	Double
The Z-coordinate value of the point #1	Double
The surface information of the intersection point #2	String
The X-coordinate value of the point #2	Double
The Y-coordinate value of the point #2	Double
The Z-coordinate value of the point #2	Double

The intersection points on lateral surfaces	
The probable intersected discontinuities	String
The number of intersection points on lateral surface	Integer
The X-coordinate value of the point #1	Double
The Y-coordinate value of the point #1	Double
The Z-coordinate value of the point #1	Double
The X-coordinate value of the point #2	Double
The Y-coordinate value of the point #2	Double
The Z-coordinate value of the point #2	Double

Figure 3. ER diagram of designed database.

A rock mass mapping model is able to calculate the coordinates of the intersection point (vertex) between the edge of a representing prism-discontinuity trace and discontinuity trace-discontinuity trace for all discontinuity data. This data can also generate a discontinuity surface in the rock mass with the representing prism (Figure 4a). Equation 1 is used in all the intersection calculations, considering the possible conditions of spatial positions of a discontinuity surface. A possible surface may form at least three vertices and at most six vertices (edge-discontinuity trace intersection) on the boundary of the representing prism. The surface can be determined by strolling on the vertex with respect to the possible orientations of surfaces (Figure 4b). The data pertaining to the vertex points of the discontinuity surfaces are recorded in *The Vertex Points of Discontinuity Surfaces Table*. Each discontinuity forms a plane of discontinuity. For this reason, *The Vertex Points of Discontinuity Surfaces Table* stores the discontinuity number, number of vertices forming the discontinuity plane, and coordinate values of each vertex. The related values in this table are presented as fields in Figure 3.

The field *The Axis of Discontinuity Surface* in *The Vertex Points of Discontinuity Surface Table* is the discontinuity trace extent drawing the order of discontinuity edges on the representing prism. The field content is produced according to the procedures shown in Figure 4a (the representing prism surfaces are denoted +X, –X, +Y, –Y, +Z, and –Z). In the examples involving the minimum (three) and maximum number (six) of vertices, the strings +Z + Y – X and +Z + X + Y – Z – X – Y represent the first and second discontinuities, respectively (Figure 4b).

The dip and dip direction angles of the discontinuity surface determine which discontinuity trace is on each representing prism surface. Thus only one intersection point exists between two discontinuity traces on any surface of a representing prism, and two intersection points exist between two discontinuity surfaces on any double surface of a representing prism. For example, for two discontinuity surfaces that have dip angles greater than and less than 90°, respectively, the human eye can clearly perceive the intersection points, line, and discontinuity surfaces. However, a computer code cannot do so itself. Therefore, an appropriate approach should be developed. In the developed approach, it is preferred to search for the existence of possible intersection points on all the representing prism surfaces by comparing each discontinuity surface with other possible discontinuity surfaces. If the Axis of Discontinuity Surface (in *The Vertex points of Discontinuity Surface Table*) field features the same surface data for both discontinuity traces on the same representing prism surface, the two traces are on the same representing prism surface. Thus the possibility of an intersection can be considered. Therefore, the main problem can be reduced to one involving the intersection of two straight lines.

First, it is determined whether two discontinuity traces on the same surface are parallel to each other. The case of parallelism can be described as follows:

1) Let the initial point and end point of the first discontinuity be i (x_i, y_i) and j(x_j, y_j), respectively.

2) Let the initial point and end point of the second discontinuity be k (x_k, y_k) and l (x_l, y_l), respectively (Figure 5b).

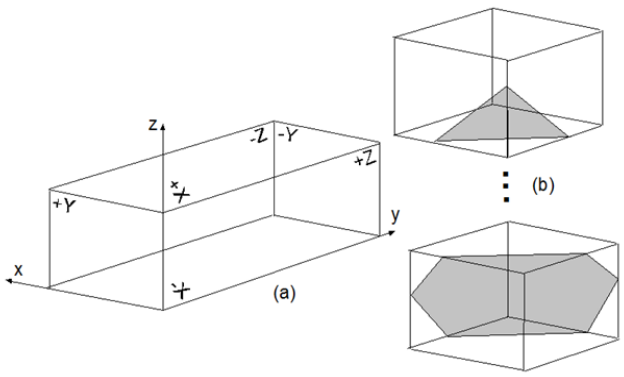

Figure 4. Representing prism and example of surfaces inside it: a) all representing prism surfaces; b) formed minimum (three) and maximum (six) vertices.

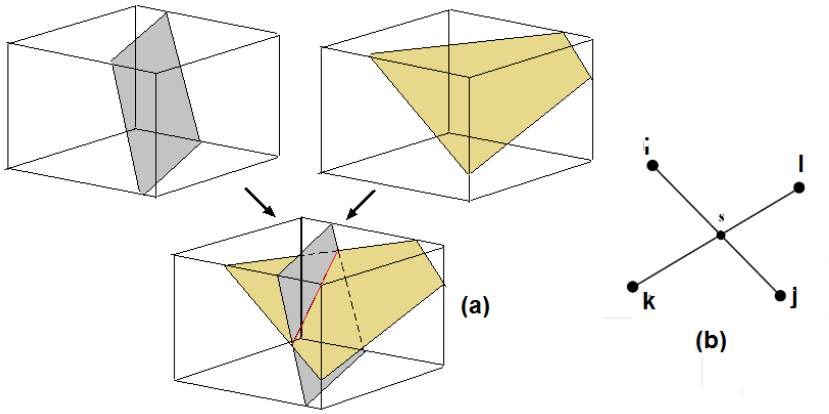

Figure 5. a) Example of intersection between two surfaces. b) Initial and end points of discontinuities on visible surface.

The parameter d in Equation 2 must be calculated to test for parallelism.

$$d = (x_j - x_i)(y_k - y_i) - (x_k - x_i)(y_j - y_i) \quad (2)$$

If $d = 0$, there are *no intersection points* between these two straight lines (the lines are *parallel*); otherwise, the parameters p_1 and p_2 are calculated using Equations 3 and 4, respectively, as 2-D coordinate points.

$$p_1 = \frac{(x_k - x_i)(y_i - y_k) - (x_i - x_k)(y_k - y_i)}{d} \quad (3)$$

$$p_2 = \frac{(x_i - x_k)(y_j - y_i) - (x_j - x_i)(y_i - y_k)}{d} \quad (4)$$

If $0 \le p_1 \le 1$ and $0 \le p_2 \le 1$, the intersection point is on these two discontinuity traces. Thus the coordinates of the intersection points can be calculated using Equations 5 and 6.

$$x_s = x_i + p_1(x_j - x_i) \quad (5)$$

$$y_s = y_i + p_1(y_j - y_i) \quad (6)$$

These equations can be calculated only on 2-D planes. Equations 5 and 6 are valid for the same representing prism surfaces. If the intersection point is searched for on the front or back (+Z or –Z) vertical surface, the x-coordinates are not considered. Similarly, if the intersection point is searched for on the upper or base (+X or –X) horizontal surface, the z-coordinates are not considered, and if the intersection point is searched for on the lateral (+Y or –Y) vertical surface, the y-coordinates are not considered.

This search process is repeated for the remaining representing prism surfaces. The results for all the representing prism surfaces are saved in three different tables: *The Intersection Points on Lateral Surfaces, The Intersection Points on Outcrop*, and *The Intersection Points on Upper Surfaces*. These three tables can be reduced to a single one: *The Intersection Table*. If two consecutive discontinuity planes have an intersection, the intersection points can be cut 1 or 2 times on each opposing face of the prism. It is also possible that the prism will never cut off each opposing face. In this case, the intersections may not be on the opposite faces but on the neighbouring faces. The number of intersection points in the generated tables represents this number of cuts for each opposing face. In the tables, 1 or 2 vertex coordinate values are stored according to the number of cuts. In addition, IDs of the intersecting discontinuities are stored in the text form. The field structures of the reduced table and the three separate tables are presented in Figure 3.

2.5. Scatter points, intersection lines, and failure modes

In developing our proposed method, assumptions for factors other than the rigidity of blocks were made. In particular, the discontinuities were considered to be linear, infinite, and randomly-oriented; the interior friction angles on the discontinuity surfaces were assumed to be the same, and a maximum of two straight lines (discontinuity trace-discontinuity trace or discontinuity trace-representing prism edge) were considered to intersect at only one point. Therefore, the obtained intersection points and straight lines (intersection line) passing through two intersecting points, which represent the boundaries of a polyhedral rock block, were used as the input data for the 2-D and 3-D visualizations. In addition, only the spatial-geometric relationships of discontinuities were examined. All the modelling processing

steps were carried out on a selected representing rectangular prism.

Determination of the angles of intersection lines between the excavation surface and other surfaces of the representing prism is an important step. This process involves a series of trigonometric calculations to solve the angles and lengths of the intersecting lines. All the discontinuity intersection data are obtained from a spreadsheet file generated by the Linear Isometric Projection of Rock Mass (LIP-RM) software [53]. The data is filtered using a logical order in the MATLAB R2014b environment so that the sliding and toppling intersections can be classified separately. With this filtering process, the slopes and the slopes of the cutting edges are compared; the slopes leaning in the same direction and the slopes leaning in the opposite directions are separated.

The scatter points are the intersecting points between two discontinuity traces. They are created simply from the coordinates of the intersection of two discontinuity traces on the excavation surface. These secondary data are used in the following statistical analysis steps.

In the model, two angular conditions from the slope, the intersection line, and the interior friction angle are taken into account to consider the occurrence of *failure modes*:

a) The first condition is that the angles of the intersection lines and surfaces have smaller values (for wedge and plane) than the dip angle of the slope, and the angle of the intersection lines and surfaces must be greater than the friction angle for the occurrence of failure. This condition can be expressed as $\psi_{fi} > \psi_i > \phi$ *for sliding failures.*

b) The second condition is that $\psi_{fi} > (90° - \psi_i) + \phi$ only for the toppling failures (Goodman and Bray 1976) [47]. The cross-section geometry of a slope exhibiting a failure can be detailed according to the three failure modes shown in Figure 1. In this definition, the dip angle of the intersection is measured clockwise.

In the model used in this work, all the intersection angles were treated as acute angles for simplicity (the dip angle of intersection for toppling was converted to an acute angle). Furthermore, without referring to these definitions, only discontinuities with a reverse angle relative to the slope dip were modelled to develop a more general approach (Figure 1c). In addition, several ranges of friction angles were selected. Thus the intersection lines and points identified fell within these ranges.

The main aim of data visualization is to communicate information clearly and efficiently to the user via statistical graphics, plots, information graphics, and tables. To this end, the 2-D and 3-D visualizations of intersection lines and the K-means of intersection points were generated.

2.6. Clustering process and K-means method

The aim of a spatial point pattern analysis is to represent any characteristic of a rock mass. In this work, highlighting weak zones on a rock slope was essentially achieved using the K-means clustering algorithms. Clustering involves grouping similar objects together in a set. Clustering analysis is a common well-known data mining and statistical data analysis method. There are several clustering methods [54-56] such as the expectation maximization, decision tree, neural network, K-means, C-means, and K-medoids methods. The oldest, simplest, and most common one is *K-means*, an algorithm that groups objects into a constant *k* number of clusters. Another soft computing clustering algorithm is *fuzzy K-means*, also known as *smooth K-means*, which differs slightly from the K-means algorithm. Objects are members of distinct clusters in which an object can only belong to one cluster in the K-means algorithm, whereas objects are the weighted members of every cluster in the fuzzy K-means algorithm. In the fuzzy K-means method, membership of an object to any group is defined by a scalar value. In our experimental study, the K-means and fuzzy K-means methods yielded similar results. Therefore, only the K-means output was considered in the case study. The K-means method can be explained briefly as what follows.

Given a set of observations ($a_1, a_2, \ldots, a_n$), where each one is a *d-dimensional* real vector*, K-means* clustering aims to partition the *n* observations into k ($\leq n$) sets $S = \{S_1, S_2, \ldots, S_k\}$ in order to minimize the within-cluster sum of squares. Formally, the objective is to find [57]:

$$arg_S\, min \sum_{i=1}^{k} \sum_{a \in S_i} \|a - \mu_i\|^2 = arg_S\, min \sum_{i=1}^{k} |S_i|\, Var S_i \quad (7)$$

where μ_i is the mean of points in S_i. This formulation is equivalent to minimizing the pairwise squared deviations of points in the same cluster:

$$arg_S\, min \sum_{i=1}^{k} \frac{1}{2|S_i|} \sum_{a,b \in S_i} \|a - b\|^2 \quad (8)$$

Since the total variance is constant, this formulation is also equivalent to maximizing the squared deviations between points in different clusters [57].

The clustering method divides the given *n* number of objects into a specific number of groups. Each group represents a cluster; each object belongs to any one of the groups. Each group may be represented by a *centroid* or *cluster* representative. The most important step in developing this type of algorithm is to define the *k* constant number of clusters (or centroid number). The elbow method (also called the knee method) has been widely used to validate the number of clusters for many statistical data analyses. This heuristic method, which looks at the percentage of variance explained as a function of the number of clusters (appropriately determining the Elbow point), was used in this work to determine the critical failure zones according to the given friction angle ranges.

2.7. Wedge structure

The formation and identification of locations with the centroids of wedges (as one of the final solutions) on a slope surface involves a series of filtering processes. The intersection points calculated by LIP-RM may be found both within the rock mass and on the surfaces. There are also 4 points (two of them on the crest and the other two must lie on the excavated (+Z) and upper (+X) surface of the slope) for constructing the wedge form. Filtering eliminates the intersection points within the slope. The process also selects the identified 4 points that form the wedge condition. In other words, the basic principle for defining wedges in the model is to identify the day-lighted tetrahedrons because not all tetrahedrons may be day-lighted. A side view of a wedge, with its components used in the model, is presented in Figure 1b.

2.8. Tool, environment, and flow diagram used to assess stability of a rock slope

In order to determine the block geometry in 2-D and 3-D, a computer code was developed to calculate the coordinates of the block vertices in the rock mass and to introduce a graphical survey of rock mass faces into the MATLAB R14 environment. The LIP-RM software and the newly developed computer code were used to prepare the database and visualizations of the rock mass. These processes can be regarded as query operations, which request several pieces of data from a database, obtained from the LIP-RM code. The developed code is capable of processing data and visualizing the calculated secondary data, separately. The complete flow diagram of the developed code is presented in Figure 6.

3. Field experiment

Highway rock cut at 20 km on the Seydişehir-Antalya road wall in Turkey was chosen for the field experiment. In this region, the main formation is composed of limestone. The experimental rock slope contains bedding and joints that can be easily observed in the field. In particular, block failures and individual wedges have often been encountered during the precipitation seasons in the region. The experimental outcrop on which the data was recorded is shown in Figure 7a. The scan-line height was taken as 1 m in the measurement studies. The outcrop dip and dip direction were recorded as 85° and 274°, respectively. The dimensions of the sampled prism dimensions were defined as (x, y, z) = (30 × 140 × 12) m. For the field experiment, 125 discontinuities were recorded, as shown in Table 1 (in sample). The output of the 3-D discontinuity planes obtained by running the LIP-RM software is shown in Figure 7b.

The developed code is capable of constructing several visualizations. In this work, a different strategy was developed and incorporated into the model, and the code was tested on the chosen field. From the first to the last step, the model deploys an increasingly detailed analysis to consider the stability problem. As the model runs, more basic sub-results can be obtained; the final results will be presented only for current locations of the experimental rock slope. The results of the model are presented as 2-D plane views and 3-D intersection lines, scatter points, K-means of intersection points, and location of intensities (as centroids) of the two main groups of the dip angle of discontinuity in k-means clustering.

To demonstrate the changes in the results of the model, five friction angle ranges were selected: $\psi_{fi} > \psi_i > \phi \geq 0°$, $\psi_{fi} > \psi_i > \phi \geq 20°$, $\psi_{fi} > \psi_i > \phi \geq 35°$, $\psi_{fi} > \psi_i > \phi \geq 55°$, and $\psi_{fi} > \psi_i > \phi \geq 75°$. These ranges were selected regardless of the type of rock and other properties of the discontinuity surface. The ranges can be narrowed or extended, and the number of ranges can be increased or decreased.

Furthermore, for a planar, clean (no infilling) discontinuity, the cohesion will be zero, and the shear strength will be defined solely by the interior friction angle. A typical range of friction

angles for a limestone discontinuity has been reported to be 34° – 40°(classified as high friction) by Barton (1973) [58]. This range approximately corresponds to the selected range of $\psi_{fi} > \psi_i > \phi \geq 35°$. This is assumed as the key range for assessing a rock slope.

The results of the wedge analyses are presented as 3-D wedges, scatter points, K-means of intersection points (only in the ranges of $\psi_{fi} > \psi_i > \phi \geq 0°$ (all wedges) and $\psi_{fi} > \psi_i > \phi \geq 35°$ (critical wedges)), and locations of intensities as centroids.

In addition, the result of the intersecting lines whose dip direction is greater than 70° is presented for toppling failures.

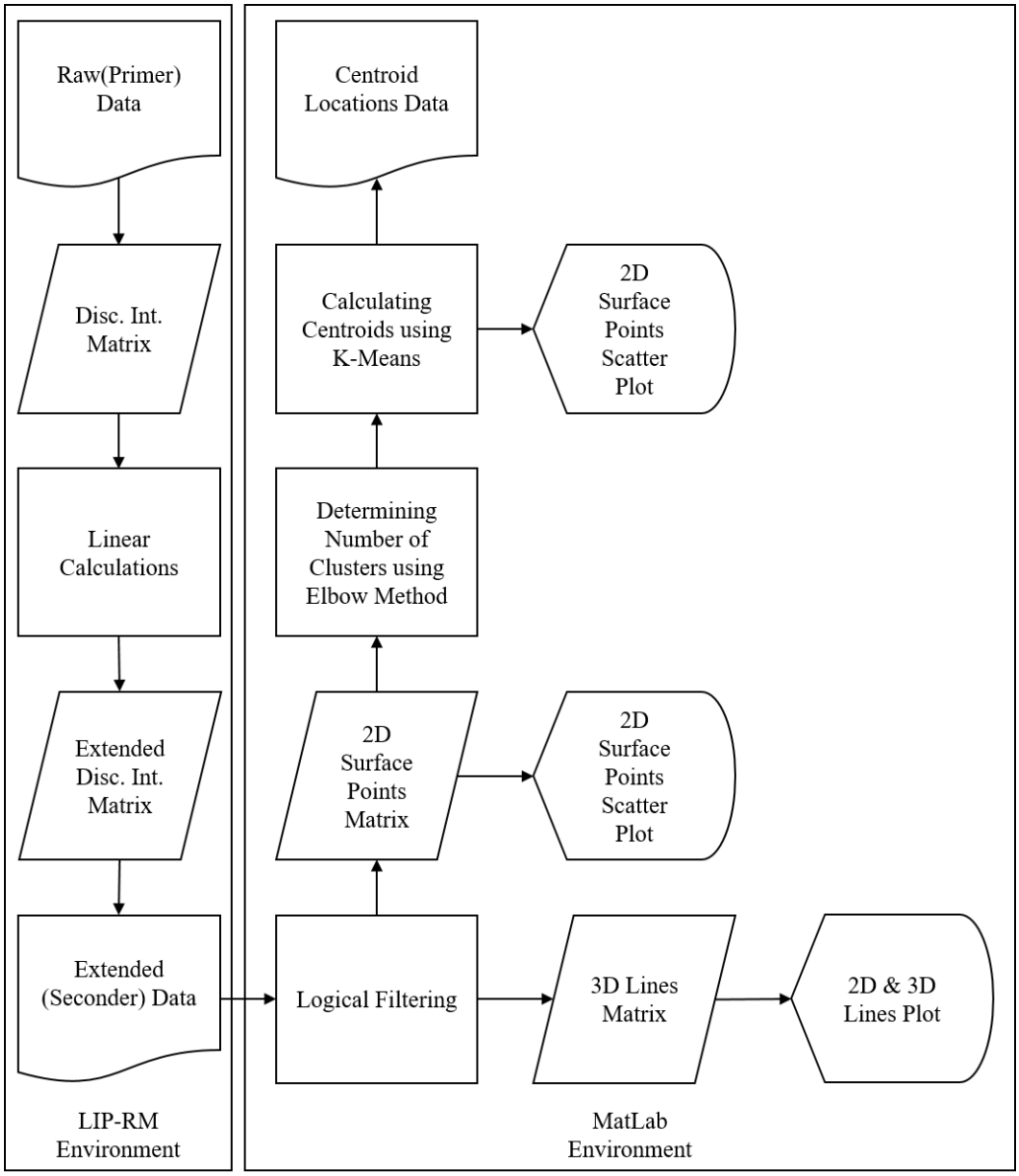

Figure 6. Flow chart of model implementation.

Table 1. Input data for experimental slope.

Discontinuity Number	Cumulative Spacing (m)	Spacing (m)	Dip (°)	Dip Direction (°)
1	0.6	0.6	59	311
2	1.78	1.18	61	309
3	1.89	0.11	64	25
. . .	. . .	. . .	. . .	. . .
123	137.55	0.45	21	332
124	138.7	1.15	25	332
125	139.4	0.7	22	338

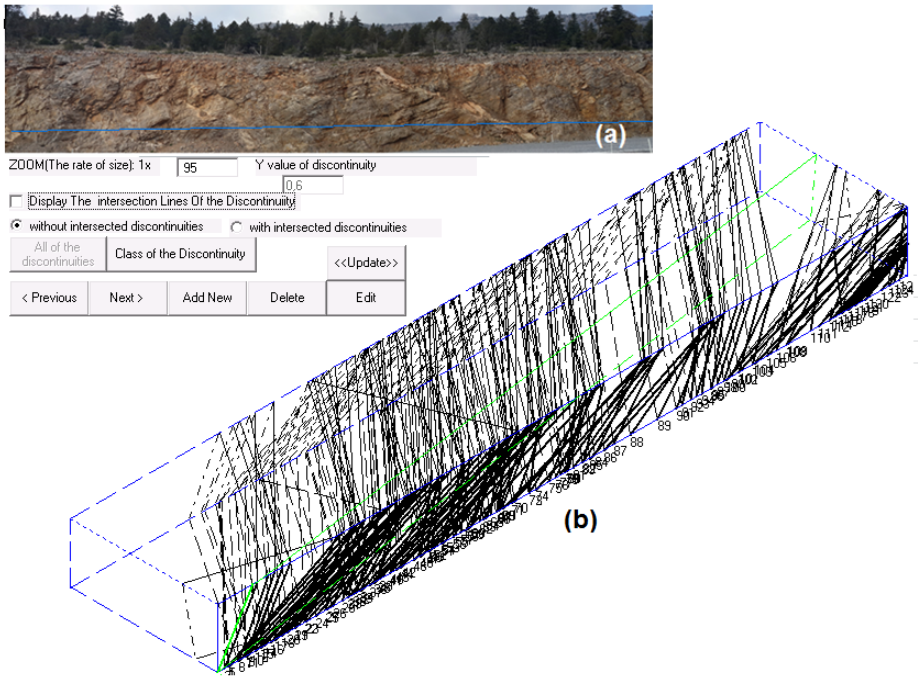

Figure 7. a) Studied highway slope that formed limestone (blue line indicates approximate scan-line through +y direction); b) image capture of experimental rock slope obtained by LIP-RM.

3.1. Results of experimental rock slope

The visual results obtained for the experimental rock slope in the current location are displayed as follow:

a) A 3-D model of the rock slope with all the intersection lines without any exclusion in Figure 8,

b) A 3-D model of the rock slope with only the daylight intersection lines on the excavating surface in Figure 9,

c) A 2-D analysis of the intersecting lines in the reverse direction compared with the excavating surface and details in Figure 10,

d) A 2-D analysis of the intersecting lines in the same direction compared with the excavating surface on the excavating surface and details in Figure 11,

e) All wedge structures on the excavating surface of the experimental slope and details in Figure 12,

f) The wedge structure on the excavating surface of the experimental slope in the range of $\psi_{fi} > \psi_i > \phi \geq 35°$ and details in Figure 13,

g) An analysis of the dip of intersecting lines greater than 70° (drop in $\psi_{fi} > \psi_i > \phi \geq 35°$ range) and details in Figure 14,

h) Numerical results of the experimental rock slope in Table 2.

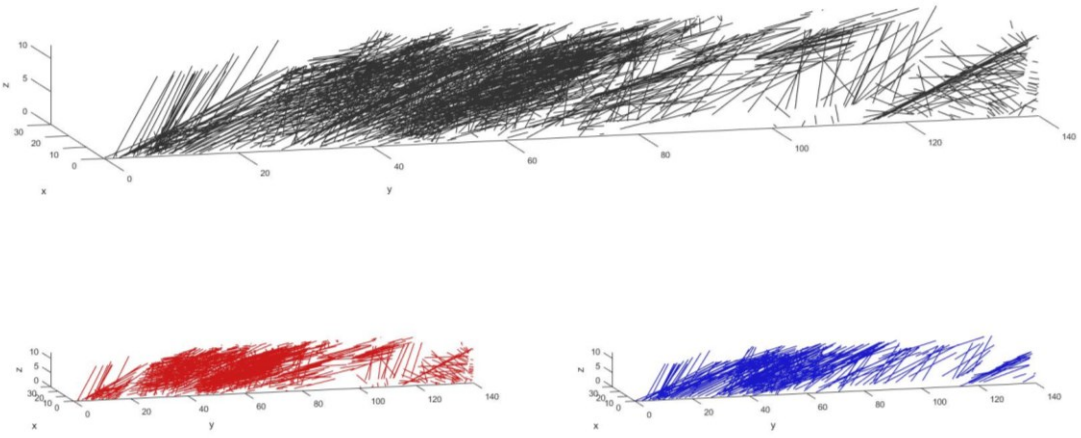

Figure 8. 3-D modelling of rock slope with a) all intersection lines without any exclusion (920); b) intersection lines in reverse direction compared with slope direction (661); c) intersection lines in the same direction compared with slope direction (259).

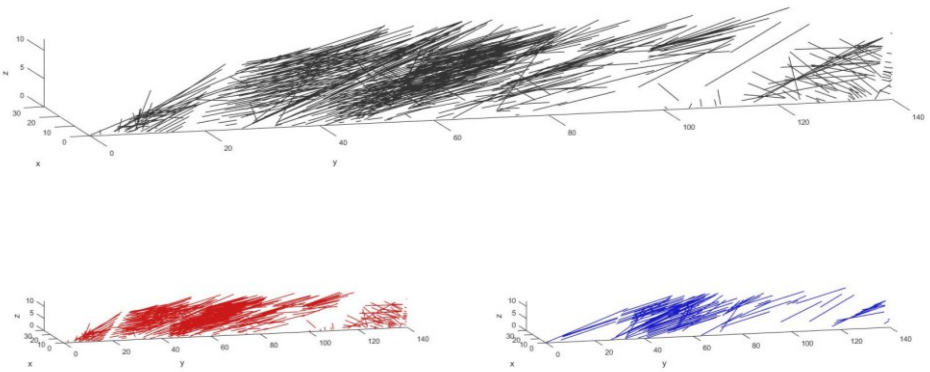

Figure 9. 3-D modelling of rock slope with only daylight intersection lines on excavating surface: a) intersection lines without any exclusion (556); b) intersection lines in reverse direction compared with slope direction (447); c) intersection lines in the same direction compared with slope direction (109).

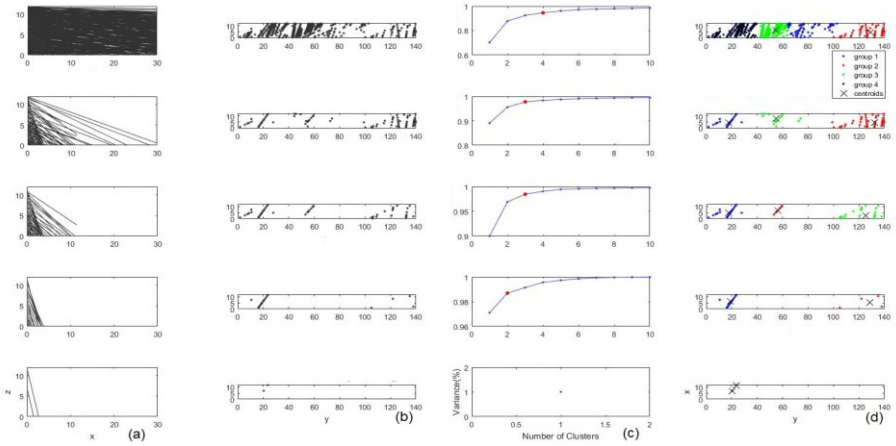

Figure 10. 2-D analysis of intersecting lines in reverse direction compared with excavating surface: a) view of intersection lines on +y surface (see Figure 3a); b) scatter point plots; c) number of centroids (elbow solution); d) K-means (determined centroid locations on excavating surface). Rows denote general condition according to five selected friction angle ranges: 1st row: $\psi_{fi} > \psi_i > \phi \geq 0°$, 2nd row: $\psi_{fi} > \psi_i > \phi \geq 20°$, 3rd row: $\psi_{fi} > \psi_i > \phi \geq 35°$, 4th row: $\psi_{fi} > \psi_i > \phi \geq 55°$, 5th row: $\psi_{fi} > \psi_i > \phi \geq 75°$.

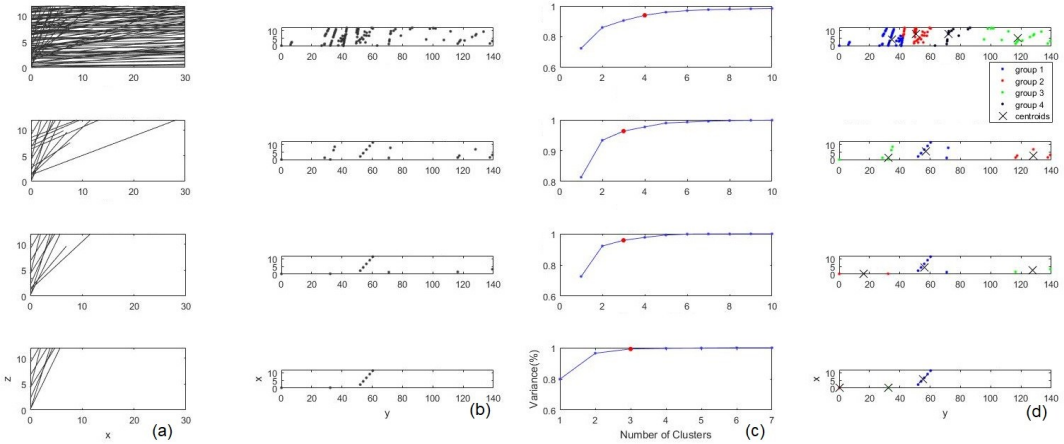

Figure 11. 2-D analysis of intersecting lines in same direction compared with excavating surface on excavating surface: a) view of intersection lines on +y surface (see Figure 3a); b) scatter point plots; c) number of centroids (elbow solution); d) K-means (determined centroid locations on excavating surface). Rows denote general condition according to five selected interior friction angle ranges: 1st row: $\psi_{fi} > \psi_i > \phi \geq 0°$, 2nd row: $\psi_{fi} > \psi_i > \phi \geq 20°$, 3rd row: $\psi_{fi} > \psi_i > \phi \geq 35°$, 4th row: $\psi_{fi} > \psi_i > \phi \geq 55°$, 5th row: $\psi_{fi} > \psi_i > \phi \geq 75°$. Note that any discontinuity was not determined in $\psi_{fi} > \psi_i > \phi \geq 75°$ range.

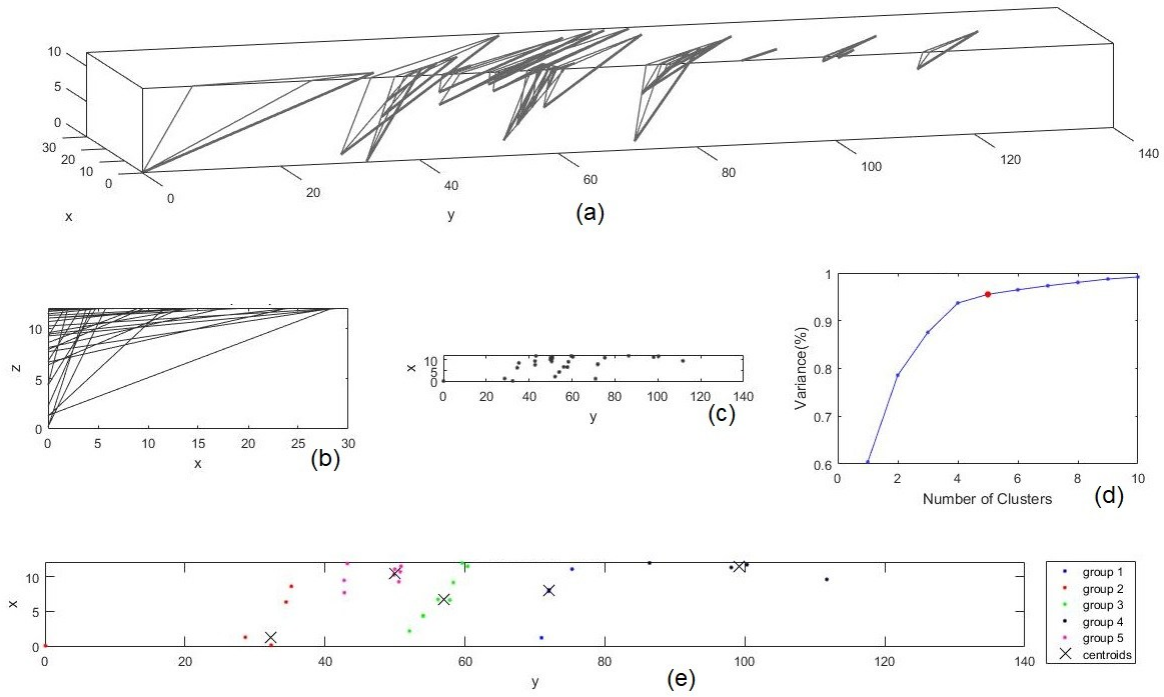

Figure 12. All wedge structures on excavating surface of experimental slope: a) 3-D plot wedges; b) view of intersection lines on +y surface (see Figure 3a); c) scatter point plots; d) number of centroids (elbow solution); e) K-means (determined centroid locations on excavating surface).

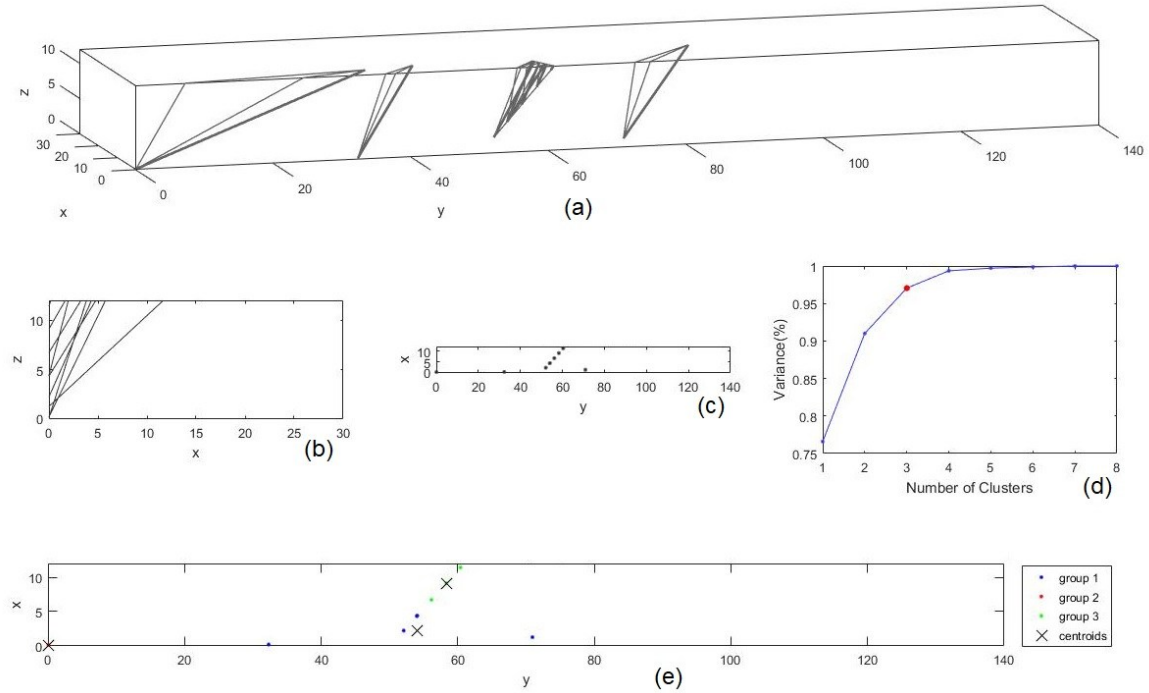

Figure 13. Wedge structure on excavating surface of experimental slope in $\psi_{fi} > \psi_i > \phi \geq 35°$ range: a) 3-D plot wedges; b) view of intersection lines on +y surface (see Figure 3a); c) scatter point plots; d) number of centroids (elbow solution); e) K-means (determined centroid locations on excavating surface).

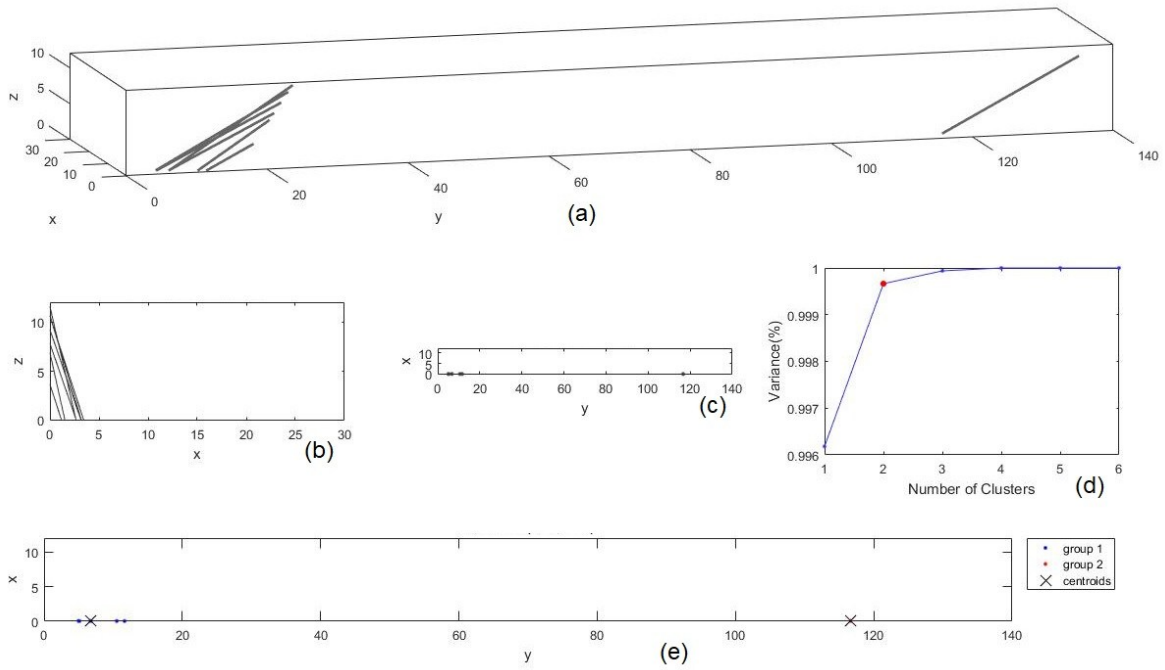

Figure 14. Analysis for dip angle of intersecting lines greater than 70° (drop in $\psi_{fi} > \psi_i > \phi \geq 35°$ range): a) 3-D intersection lines; b) view of intersection lines on +y surface (see Figure 3a); c) scatter point plots; d) number of centroids (elbow solution); e) K-means (determined centroid locations on excavating surface).

Table 2. Results for excavating surface of experimental slope.

Intersection Line Direction	Friction Angle Range (°)	Exposed Point Number	Centroid Number	Centroid Coordinate (y, z) (m)
Opposite Direction of Slope (a)	$\psi_{fi} > \psi_i > \phi \geq 0°$	447	4	(26.73, 5.64), (54.38, 6.55), (75.08, 8.57), (128.83, 4.65)
	$\psi_{fi} > \psi_i > \phi \geq 20°$	86	3	(17.70, 4.61), (55.02, 7.92), (132.18, 4.47)
	$\psi_{fi} > \psi_i > \phi \geq 35°$	48	3	(17.70, 4.61), (56.25, 6.83), (125.22, 2.54)
	$\psi_{fi} > \psi_i > \phi \geq 55°$	17	2	(19.08, 6.34), (128.53, 5.14)
	$\psi_{fi} > \psi_i > \phi \geq 75°$	2	2	(20.32, 6.89), (23.62, 11.60)
Same Direction as Slope (b)	$\psi_{fi} > \psi_i > \phi \geq 0°$	109	4	(34.65,3 .92), (50.56, 7.68), (72.21, 8.09), (117.85, 5.03)
	$\psi_{fi} > \psi_i > \phi \geq 20°$	18	3	(32.32, 1.31), (57.24, 5.57), (128.14, 2.71)
	$\psi_{fi} > \psi_i > \phi \geq 35°$	11	3	(0.07, 0.11), (55.11, 4.37), (127.87, 2.31)
	$\psi_{fi} > \psi_i > \phi \geq 55°$	8	3	(0.07, 0.11), (32.32, 0.18), (55.11, 5.57)
	$\psi_{fi} > \psi_i > \phi \geq 75°$	0	0	-
Wedges (c)	$\psi_{fi} > \psi_i > \phi \geq 0°$	29	5	(32.32, 1.31), (49.99, 10.25), (57.84, 6.72), (72.01, 7.99), (99.17, 11.50)
	$\psi_{fi} > \psi_i > \phi \geq 35°$	9	3	(0.07, 0.11), (54.00, 2.21), (58.33, 9.14)
Topplings (d)	$\psi_{fi} > \psi_i > \phi \geq 70°$	7	2	(21.47, 8.53), (135.17, 10.60)

3.2. Discussion on results

When the dip of the intersection lines that are in the reverse and the same direction is compared with the slope, the dip is assigned as flexural, block-flexure toppling (dip angle of discontinuity greater than 70°) or block toppling (sliding, toppling, and sliding-toppling modes) (see Figure 1c), and the day-lighted points are classified as individual or combinations of planar and wedge failures (see Figures 1a and 1b).

The results can be summarized as follow:

a) Forty-eight intersection points with three centroids of clusters (reverse direction compared to slope dip) and 11 intersection points with three centroids of clusters (same direction as slope dip) were defined on the excavating surface in the $\psi_{fi} > \psi_i > \phi \geq 35°$ range.

b) Twenty-nine (five centroids) and nine (three centroids) wedge structures were defined for the $\psi_{fi} > \psi_i > \phi \geq 0°$ and $\psi_{fi} > \psi_i > \phi \geq 35°$ ranges, respectively.

c) The centroids in the $\psi_{fi} > \psi_i > \phi \geq 35°$ range were assumed to represent the critical ones in terms of the failure zones.
d) The condition of the dip of the toppling surface must be greater than 70° for toppling failure, which refers to the condition $\psi_{fi} > \psi_i \geq 70°$. In this condition, only seven exposed points and two centroids with their coordinates were identified on the bottom part of the excavating surface.
e) It can be concluded that the states in the ranges $\psi_{fi} > \psi_i > \phi \geq 35°$ (c) and $\psi_{fi} > \psi_i \geq 70°$ (d) are critical in terms of the respective failure modes according to the proposed model.
f) All the obtained coordinates of the zones of weakness are consistent with the visuals generated by the model.

4. Conclusions

In this paper, a process starting from a scan-line survey and ending with the generation of visual models is presented as a sequential structure of sub-models. These sub-models can be interpreted separately for the components in the structure or as a whole. This hierarchical structure consists of the following components, with measurements simply recorded by the scan-line method. The discontinuity planes can be identified. The discontinuity intersections can be calculated as points. The scatter points and intersection lines between two discontinuities can be defined. Failure modes can be defined as two groups according to the orientation of the intersection lines. With the K-means method, different failure modes are modelled over different interior friction angle ranges, and the location of the weak zones can be determined dynamically. In addition, wedge forms, which are a common type of sliding structure over critical interior friction angle ranges, can be identified, and their locations can be determined.
According to the experimental study, 3 (wedge failure) (Table 2c) and 2 (toppling failure) (Table 2d) centroid locations in the critical friction angle ranges appear to be unstable. These results are similar to those obtained from the analysis of the intersection lines running in the opposite (Table 2a) and same direction (Table 2b), with the slopes presented along with their visualization details in Table 2.
In this work, construction of the model involved a stepwise approach for identifying the weak zones; the steps of the model are closely linked to each other. In addition, all steps involve increasing amounts of detail until the final analysis results (centroid locations) of the model are obtained. In this work, all processes were performed without any other field characterization study or mechanical tests. The dip, dip direction, and spacing measurements from the scan-line survey were sufficient to obtain the results without any other equipment.
The detailed analyses are expensive and time-consuming. In addition, in predicting the weak zones using the current model, knowing where the detailed analysis should be focused would be advantageous in terms of saving time and resources.
There is no doubt that the model cannot explain more complex failures that can be triggered by other failures or by interlocking blocks. Nevertheless, the beginning of the failure zones was successfully modelled as a basic failure mode separately; hence, the developed model can be used to predict the basic failure zones along the excavating surface of a rock slope. Thus the coordinates of the supporting measures can be defined. This method can be used in many applications of excavation engineering, from preliminary assessment to final decision steps.
Surely, there are numerous other parameters to consider as well such as water pressure, cohesion, and roughness. These parameters can be adapted to the model in the future works to provide a more detail and a higher accuracy in assessing the rock slope stability. Additionally, we plan to adopt more detailed survey methods to improve the measurement processes in the initial steps of the model.

References

[1]. Bieniawski, Z.T. (1998). Engineering rock mass classifications. John Wiley & Sons. New York. 249 P.

[2]. Hack, R.H. (1998). Slope stability probability classification. 2nd Edition. SSPC ITC. Enschede. 258 P.

[3]. ISRM. (1981). Rock characterization, testing and monitoring ISRM Suggested Methods. Pergamon. Oxford. 200 P.

[4]. Oda, M. (1980). A statistical study of fabric in random assembly of spherical granules. In: Earthquake Research and Engineering Laboratory. Technical Report. pp. 804-829.

[5]. Einstein, H.H. (1983). Probabilistic and statistical methods in engineering geology. Rock Mech. Rock Eng. 16 (1): 39-72.

[6]. Beacher, G. (1983). Statistical analysis of rock mass fracturing. Math. Geol. 15 (2): 329-347.

[7]. Hoek, E. and Bray, J.W. (1981). Rock Slope Engineering, Revised 3rd ed. The Institution of Mining and Metallurgy. London. pp. 341-351.

[8]. Davis, D.J. (2002). Statistics and Data Analysis in Geology. 3rd Edition. Willey. New York. 638 P.

[9]. Dershowitz, W.S. and Einstein, H.H. (1988). Characterizing rock joint geometry with joint system models. Rock Mech. Rock Eng. 21: 21-51.

[10]. Lei, Q., Latham, J.F. and Tsang, C.F. (2017). The use of discrete fracture networks for modelling coupled geomechanical and hydrological behavior of fractured rocks. Comput. and Geotech. 85: 151-176.

[11]. Mardia, K.V., Nyirongo, V.B., Walder, A.N., Xu, C., Dowd, P.A., Fowell, R.J. and Kent, J.T. (2007). Markov Chain Monte Carlo Implementation of Rock Fracture Modelling. Math. Geol. 39 (4): 355-381.

[12]. Dowd, P.A., Xu, C., Mardia, K.V. and Fowell, R. J. (2007). A comparison of methods for the stochastic simulation of rock fractures. Math. Geol. 39 (7):.697-714.

[13]. Xu, C. and Dowd, P.A. (2010). A new computer code for discrete fracture network modeling. Computand Geosci. 36 (3): 292-301.

[14]. Alghalandis, Y.F., Xu, C. and Dowd, P.A. (2011). A general framework for fracture intersection analysis: algorithms and practical applications. Proc, Australian Geothermal Energy Conference, Melbourne. pp. 15-20.

[15]. Jimenez, R. (2009). Fuzzy spectral clustering for identification of rock discontinuity sets. Rock Mech. Rock Eng. 41 (6): 929-939.

[16]. Riquelme, J., Abellán, A., Tomás, R. and Jaboyedoff, M. (2014). A new approach for semi-automatic rock mass joints recognition from 3D point clouds. Comput. and Geotech. 68: 38-52.

[17]. Turanboy, A. (2016). 2D visual characterisation of wedge failure types and locations on rock slopes. Environmental Earth Sciences. 75 (12): 1-15.

[18]. Kemeny, J. and Post, R. (2003). Estimating three-dimensional rock discontinuity orientation from digital images of fracture traces. Comput. Geosci. 29 (1): 65-77.

[19]. Slob, S., Van Knapen, B., Hack, R., Turner, K. and Kemeny, J. (2005). Method for automated discontinuity analysis of rock slopes with three-dimensional laser scanning. Transportation research record. Journal of the transportation research board. 1913: 187-194.

[20]. Sturzenegger, M., Stead, D. and Elmo, D. (2011). Terrestrial remote sensing-based estimation of mean trace length, trace intensity and block size/shape. Eng. Geol. 119 (3-4): 96-111.

[21]. García-Sellés, D., Falivene, O., Arbués, P., Gratacos, O., Tavani, S. and Muñoz, J.A. (2011). Supervised identification and reconstruction of near-planar geological surfaces from terrestrial laser scanning. Comput. Geosci. 37 (10): 1584-1594.

[22]. Chen, J., Zhu, H. and Li, X. (2016). Automatic extraction of discontinuity orientation from rock mass surface 3D point cloud. Computers & Geosciences. 95: 18-31.

[23]. Gigli, G. and Casagli, N. (2011). Semi-automatic extraction of rock mass structural data from high resolution LIDAR point clout. Int. J. Rock Mech. Min. Sci. 48 (2): 187-198.

[24]. Lato, M.J. and Vöge, M. (2012). Automated mapping of rock discontinuities in 3D lidar and photogrammetry models. Int. J. Rock Mech. Min. Sci. 54: 150-158.

[25]. Haneberg, W.C. (2007). Directional roughness profiles from three-dimensional photogrammetric or laser scanner point clouds. 1st Canada-U.S. Rock Mechanics Symposium. Vancouver. pp. 101-106.

[26]. Sturzenegger, M. and Stead. M.D. (2009). Close-range terrestrial digital photogrammetry and terrestrial laser scanning for discontinuity characterization on rock cuts. Eng. Geol. 106 (3-4): 163-182.

[27]. Khoshelham, K., Altundağ, D., Ngan-Tillard, D. and Menenti, M. (2011). Influence of range measurement noise on roughness characterization of rock surfaces using terrestrial laser scanning. Int. J. Rock Mech. Min. Sci. 48 (8): 1215-1223.

[28]. Oppikofer, T., Jaboyedoff, M., Blikra, L., Derron, M.H. and Metzger, R. (2009). Characterization and monitoring of the Åknes rockslide using terrestrial laser scanning. Nat. Hazards Earth Syst. Sci. 9: 1003-1019.

[29]. Slob, S. (2010). Automated rock mass characterisation using 3-D terrestrial laser scanning. Ph.D. Dissertation. Delft University of Technology. Delft. 44 P.

[30]. Riquelme, A.J., Abellán, A. and Tomás, R. (2015). Discontinuity spacing analysis in rock masses using 3D point clouds. Eng. Geol. 195: 185-195.

[31]. Sturzenegger, M., Stead, D. and Elmo, D. (2011). Terrestrial remote sensing-based estimation of mean trace length, trace intensity and block size/shape. Eng. Geol. 119 (3-4): 96-111.

[32]. Umili, G., Ferrero, A.M. and Einstein, H.H. (2013). A new method for automatic discontinuity traces sampling on rock mass 3D model. Comput. and Geosci. 51: 182-192.

[33]. Di Crescenzo, G. and Santo, A. (2007). High-resolution mapping of rock fall instability through the integration of photogrammetric, geomorphical and engineering-geological surveys. Quat. Int. 171-172: 118-130.

[34]. Oppikofer, T., Jaboyedoff, M., Pedrazzini, A., Derron, M.H. and Blikra, L. H. (2011). Detailed DEM analyses of rock scar to characterize the basal sliding

surface of active rockslides. J. Geophys. Res. F: Earth Surg. 116 (F2): 1-22.

[35]. Abellán, A., Oppikofer, T., Jaboyedoff, M., Rosser, N.J., Lim, M. and Lato, M.J. (2014). Terrestrial laser scanning of rock slope instabilities. Earth Sur. Processes Landforms. 39 (1): 80-97.

[36]. Fekete, S. and Diederichs, M. (2013). Integration of three-dimensional laser scanning with discontinuum modelling for stability analysis of tunnels in blocky rock masses. Int. J. Rock Mech. Min. Sci. 57: 11-23.

[37]. Panet, M., Vormeringer, R., Vigier, G. and Goodman, R. E. (1969). Discussion on graphical stability analysis of slopes in jointed rock. Journal of Soil Mechanics & Foundations Div. 95: 685-702.

[38]. Markland, J.T. (1972). A useful technique for estimating the stability of rock slopes when the rigid wedge sliding type of failure is expected. Imperial College Rock Mechanics Research. Report No. 19.

[39]. Goodman, R.E. (1976). Methods of geological engineering in discontinuous rocks. West Publishing. San Francisco. 484 P.

[40]. Hocking, G.A. (1976). A method for distinguishing between single and double plane sliding of tetrahedral wedges. Int. J. Rock Mech. Min. Sci. Geomech. Abstr. 13: 225-226.

[41]. Goodman, R.E. and Shi, G.H. (1985). Block theory and its application to rock engineering, Prentice Hall. Englewood Cliffs. 338 P.

[42]. Öcal, A. and Özgenoğlu, A. (1997). Determination of sliding mode of tetrahedral wedges in jointed rock slopes.Rock Mech. Rock Eng. 30: 161-165.

[41]. Goodman, R.E. and Shi, G.H. (1985). Block theory and its application to rock engineering. Englewood Cliffs, NJ: Prentice-Hall. 26 (1): 103-105.

[43]. Kliche, C.A. (1999). Rock slope stability. SME. Colorado. 253 P.

[44]. Wyllie, D.C. and Mah, C.W. (2004). Rock slope engineering, 4th ed., Spon Press. London. 456 P.

[45]. Hoek, E. and Londe, P. (1974). The design of rock slopes and foundations. In General report of Third Congress of the International Society for Rock Mechanics. Denver.

[46]. Matheson, G.D. (1983). Rock stability assessment in preliminary site investigations: graphical methods, Transport and Road Research Laboratory. Berkshire. 30 P.

[47]. Goodman, R.E. and Bray, J.W. (1976). Toppling of rock slopes. Proc. Specialty Conference on Rock Engineering for Foundations and Slopes. Colorado. pp. 201-234.

[48]. Cruden, D.M. (1989). The limits to common toppling. Can. Geotech. J. 26 (4): 737-742.

[49]. De Freitas, M.H. and Watters, R.J. (1973). Some field examples of toppling failure. Geotechnique. 23 (4): 495-514.

[50]. Owen, G.K., Robert, J.A. and Nicholas, J.C. (1998). Mechanisms of failure and slope development in rock masses. Trans. Inst. Br. Geogr. 23 (3): 353-370.

[51]. Priest, S.D. and Hudson, J.A. (1981). Estimation of discontinuity spacing and trace length using scanline survey. Int. J. Rock Mech. Min. Sci. 18 (3): 183-197.

[52]. Priest, S.D. (1993). Discontinuity analysis for rock engineering. 1st ed., Chapman & Hall. London. 473 P.

[53]. Turanboy, A. and Ülker, E. (2008). LIP-RM: an attempt at 3D visualization of in situ rock mass structures. Comput. Geosci. 2 (12): 181-192.

[54]. Silwattananusarn, T. and Tuamsuk, K. (2012). Data mining and its applications for knowledge management: a literature review from 2007 to 2012. arXiv preprint arXiv:1210.2872.

[55]. Kalra, M. and Lal, N. (2016). Data mining of heterogeneous data with research challenges. Proc. Symposium on Colossal Data Analysis and Networking (CDAN).

[56]. Pathak, B. and Lal, N. (2017). A survey on clustering methods in data mining. Int. J. Comput. Appl. 159 (2): 6-11.

[57]. Kriegel, H.P., Schubert, E. and Zimek, A. (2016). The (black) art of runtime evaluation: Are we comparing algorithms or implementations?. Knowledge and Information Systems (KAIS). 52 (2): 341-378.

[58]. Barton, N. (1973). Review of a new shear strength criterion for rock joints. Eng. Geol. 7 (4): 287-332.

ارائه‌ی رویکردی جدید برای ارزیابی پایداری شیب‌های سنگی با توجه به مرکزیت‌های مناطق ضعیف

A. Turanboy[1*], E. Ülker[2] and C.B. Küçüksütçü[3]

1- Mining Engineering, Seydişehir Ahmet Cengiz Engineering Faculty, Necmettin Erbakan University, Konya, Turkey
2- Computer Engineering, Engineering Faculty, Selçuk University, Kampüs, Konya, Turkey
3- BayE Information, Education and Consulting Ltd., Konya, Turkey

ارسال ۲۰۱۷/۷/۷، پذیرش ۲۰۱۷/۹/۲۳

* نویسنده مسئول مکاتبات: *aturanboy@konya.edu.tr*

چکیده:

خطوط تقاطع بین سطوح ناپیوستگی و نقاط تقاطع آن‌ها بر روی سطوح قابل مشاهده هر ساختار مهندسی ممکن است شاخص‌های بی‌ثباتی باشد. در این مقاله یک رویکرد جدید برای مدل‌سازی خطوط متقاطع و نقاطی که ارزیابی اولیه از هر نوع ناپایداری را در یک ساختار مهندسی مشخص شده توسط حالت‌های شکست ارائه می‌دهد، بیان می‌کند. در این کار پژوهشی، خطوط تقاطع با توجه به جهت اصلی یا در جهت معکوس و با توجه به شیب‌شان دسته‌بندی شدند. علاوه بر این، خطوط تقاطع با توجه به محدوده‌های مختلف زاویه اصطکاک داخلی گروه‌بندی می‌شوند که می‌توانند توسط کاربر در یک برنامه کامپیوتری که برای این کار طراحی شده است انتخاب شوند. جهت‌گیری خطوط متقاطع و محل نقاط تقاطع ظاهری تعریف و به عنوان نقاط پراکندگی اختصاص داده شده است. این نقاط ظاهری برای تعیین مکان‌های مرکزی خوشه‌بندی شده‌اند که خوشه‌بندی K میانگین در این مرحله استفاده می‌شود. در نهایت، تمام این تحلیل‌ها به ترتیب منطقی یکپارچه می‌شوند و نتایج به دست آمده برای ارزیابی ناپایداری‌ها بر روی سطح شیب استفاده می‌شود. آزمایش‌ها برای نشان دادن عملکرد و نتایج این رویکرد بر روی امتداد یک برش سنگی در بزرگراه کونیا- آنتالیا (ترکیه) انجام شد که این برش سنگی از سنگ آهک ساخته شده است. مکان‌های مناطق احتمالی شکست در محدوده بحرانی زاویه اصطکاک داخلی به صورت بصری و عددی در طول شیب تعریف می‌شود. آزمایش‌های انجام شده نشان می‌دهد که روش پیشنهادی بسیار مفید و آسان برای پیاده‌سازی است و نتایج ارزیابی اولیه عملی، ناپایداری را با توجه به حالت‌های شکست اولیه ارائه می‌دهد.

کلمات کلیدی: توده سنگ، حالت‌های شکست، خطوط و نقاط تقاطع، خوشه‌بندی K میانگین، زاویه اصطکاک داخلی.